CHAPTER SIX

RESULTS

The results for the three change detection methods presented in the previous chapter as well as the EKF framework proposed in chapter 4 are shown in this chapter. The procedure for identifying ground truth data which are used for training and validation is also shown.

6.1 IDENTIFYING EXAMPLES OF SETTLEMENT DEVELOPMENT

In any change detection method, representative examples of change and no-change are necessary for not only training (supervised methods) but also for validation of the change detection method. Examples of confirmed settlement developments and no-change areas were obtained by means of visual interpretation of high resolution Landsat and SPOT5 images of 2000 and 2008 respectively. The following sections shows how the ground truth examples of no-change natural vegetation and settlement MODIS pixels as well as examples of MODIS pixels that transitioned from natural vegetation to settlement were identified.

6.1.1 Identification of change pixels

The extraction of the MODIS ground truth pixels which transitioned from natural vegetation in 2000 to settlement by 2008, was done using a six-step process. A graphical representation of each step is shown in Figure 6.1. During the first step, the SPOT5 imagery of Limpopo were used to identify human settlements. On-screen digitizing was done by manually creating a polygon along the outer edge of each settlement area (Step 2). This settlement polygon was then displayed on a co-located Landsat image from 2000 (Step 3). If the settlement polygon identified in 2008, was covered by natural vegetation in 2000, the polygon is labeled as "changed". The next step was to extract the MODIS pixels corresponding to the area covered by the change polygon. This was done by overlying the change polygons on a MODIS grid and identifying all MODIS pixels that intersect the change

Step 1

Step 2
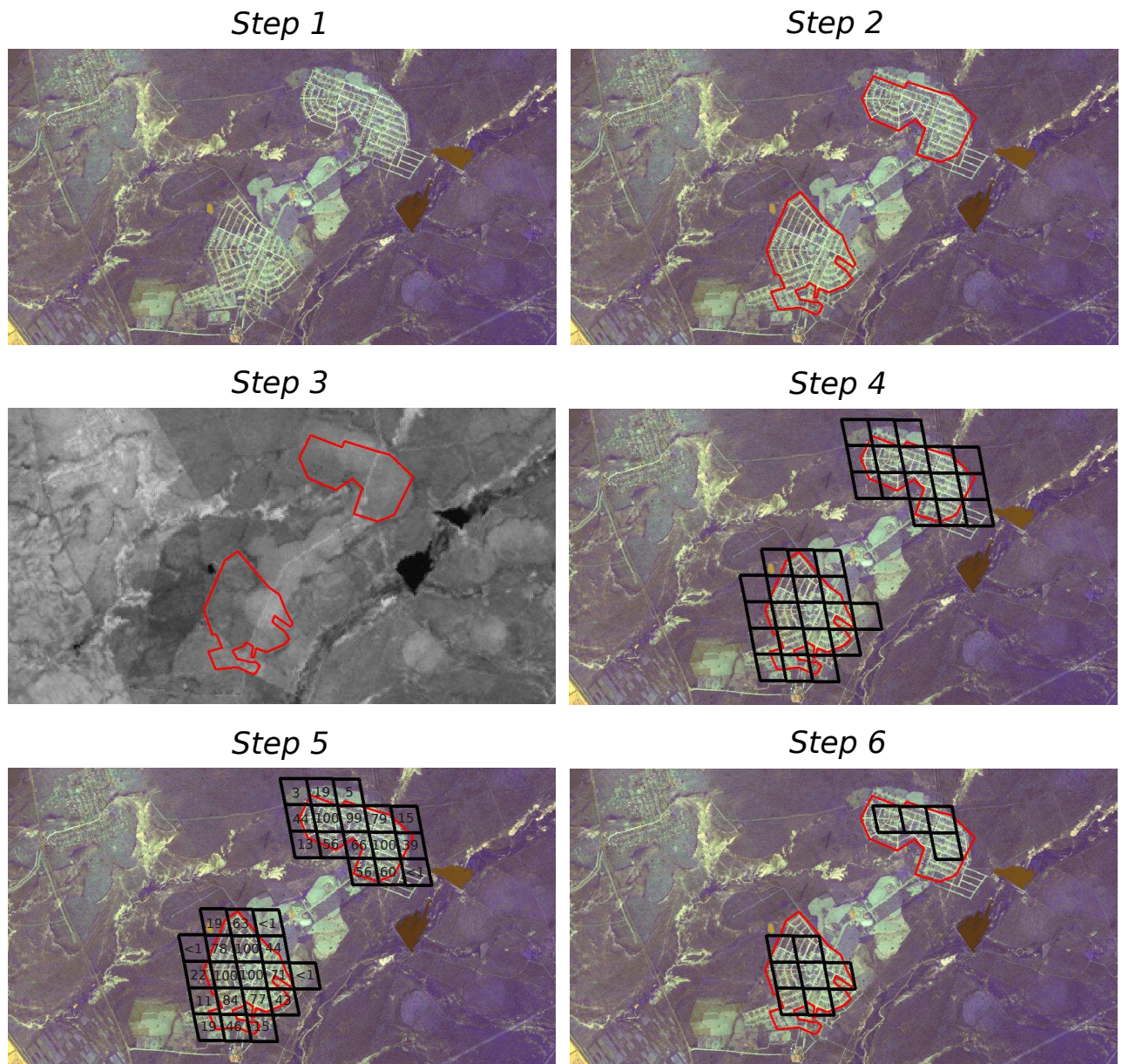
Step 3

Step 4

Step 5

Step 6

FIGURE 6.1: Graphical representation of the six steps used to identify MODIS pixels that changed from natural vegetation to settlement.

polygons (Step 4). The next step was to determine the percentage overlap between the settlement polygon and intersecting MODIS pixels (step 5). Step 5 of Figure 6.1 illustrates the percentage of polygon area intersecting each MODIS pixel. The final step was to identify the MODIS pixels that are covered by at least 70% of the change polygon, which yields the final set of MODIS pixels which changed from natural vegetation to settlement.

6.1.2   Identification of no-change pixels

The procedure for identifying no-change settlement MODIS pixels is very similar to the procedure described in the previous section with the only difference being step 3. If the Landsat 2000 image shows that the settlement polygon identified in 2008 corresponds to a settlement area in 2000, the polygon is classified as being a "no-change" settlement polygon. The procedure for extracting the corresponding MODIS pixels was done using steps 4 to 6 described in the previous section. The procedure for identifying no-change natural vegetation pixels is also conceptually similar. Representative natural vegetation areas were identified throughout the study area using the 2008 SPOT5 imagery. Polygons were created manually by means of on-screen digitization. These polygons were compared to co-located Landsat imagery in 2000 to ensure land-cover class consistency. Once the "no-change" natural vegetation polygons were identified, the process of extracting the corresponding MODIS pixels was performed using steps 4 to 6 as described in section 6.1.1.

6.1.3   Validation of MODIS pixels using Google Earth

High resolution satellite imagery in Google Earth are being used more routinely in the validation of land cover products [104]. As a validation procedure, the MODIS pixels identified during the process given in sections 6.1.1 and 6.1.2 were investigated in Google Earth using QuickBird imagery of multiple dates (Figure 6.2). The true color, high resolution QuickBird images from Google Earth proved very useful when inspecting the class membership of MODIS pixels at different time-instances. The only problem with using Google Earth for validation is that certain areas are imaged more regularly than other areas and thus multiple images are not available everywhere. This implies that in certain areas only one image was available which does not provide any information on the land cover change history of MODIS pixels.
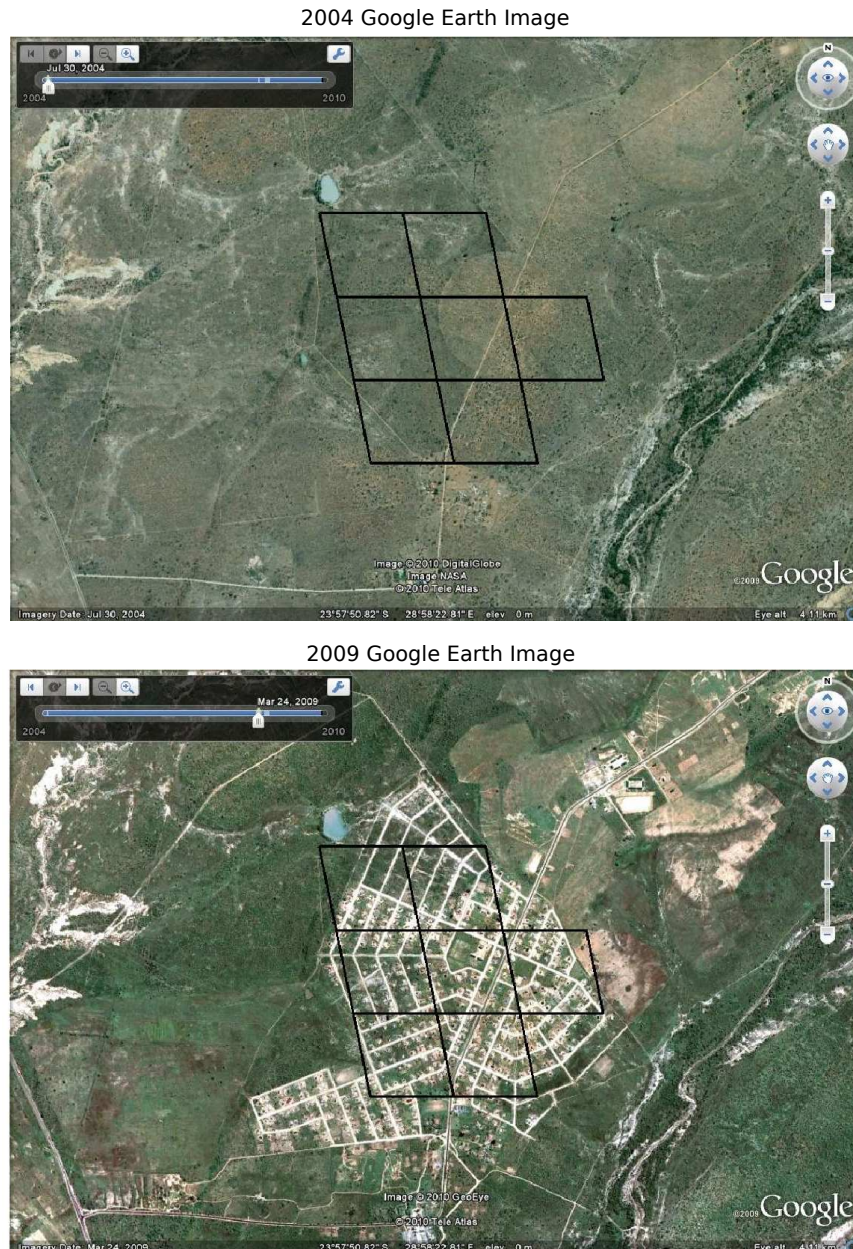
2004 Google Earth Image

2009 Google Earth Image

FIGURE 6.2: Validating MODIS pixels using QuickBird imagery at different dates (courtesy of Google^{TM}Earth).

6.2 IMPROVING   CLASS   SEPARABILITY   USING   AN   EXTENDED KALMAN FILTER

6.2.1 Study area used for testing class separability

The methods introduced in chapter 4 were tested in two regions in the Limpopo province. The first study area (Region A) is centered around latitude $24°17'21.43''$S and longitude $29°39'42.96''$E and is 43 km south east of the city of Polokwane. Region A covers a geographic area of approximately 190 km^2,
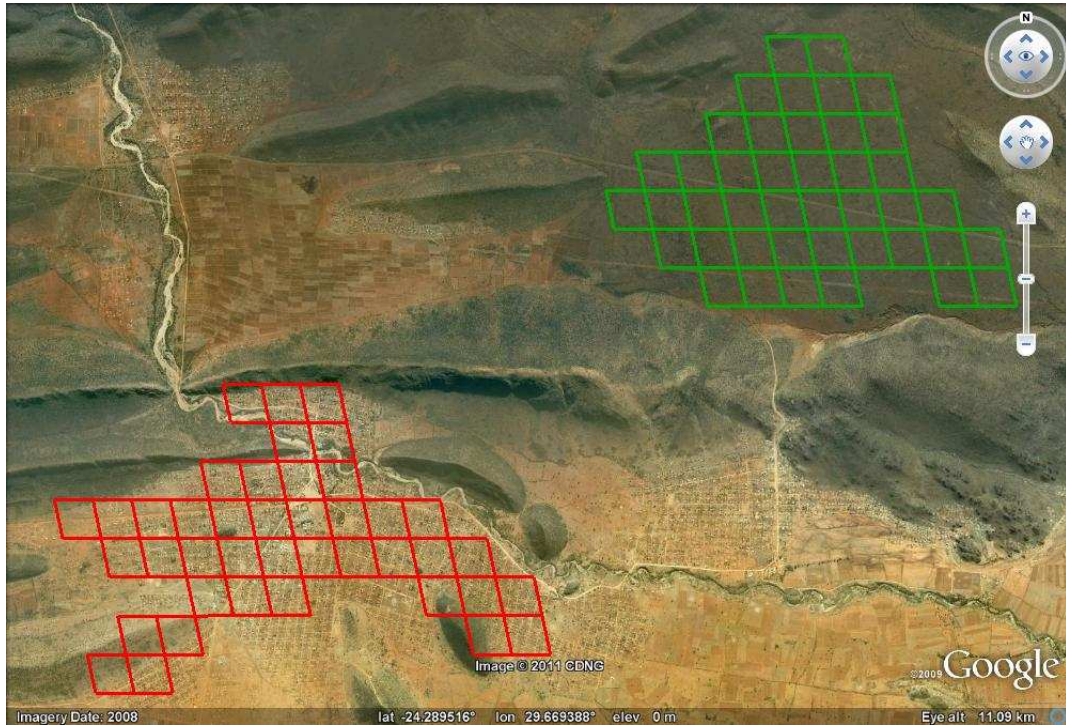
FIGURE 6.3: QuickBird image of Region A together with the MODIS pixels corresponding to the natural vegetation and settlement areas (courtesy of Google$^{\text{TM}}$Earth).

42 natural vegetation and 42 settlement pixels were selected for analysis. Region B is centered around latitude $24°19'51.50''$S and longitude $29°18'04.07''$E and is 47 km south west of the city of Polokwane. Region B covers a geographical area of 100 km^2, 32 settlement and 61 natural vegetation pixels were selected. The study regions that were considered had settlements and natural vegetation areas in close proximity which ensured that the rainfall, soil type and local climate were similar. Figure 6.3 shows the MODIS pixels that where selected for region A. Each of the MODIS pixels were evaluated using SPOT5 high resolution data to ensure that none of them had experienced any land-cover change during the study period (Section 6.1).

6.2.2   Separability results and discussion

To recap from chapter 4, the separability between two arbitrary NDVI time-series can be determined by comparing the spectral characteristics of the two time-series by making use of the FFT. In particular, the distance between the first and annual FFT components are calculated which produces a scalar quantity in each case. Based on these distance metrics, the similarity between two NDVI time-series are quantified. When using the EKF to estimate the μ and α parameter sequence for each NDVI time-series, the difference between the parameter sequences fluctuates over time. This is illustrated in figure 6.4 where the μ sequence estimated using the EKF is shown along with the FFT mean
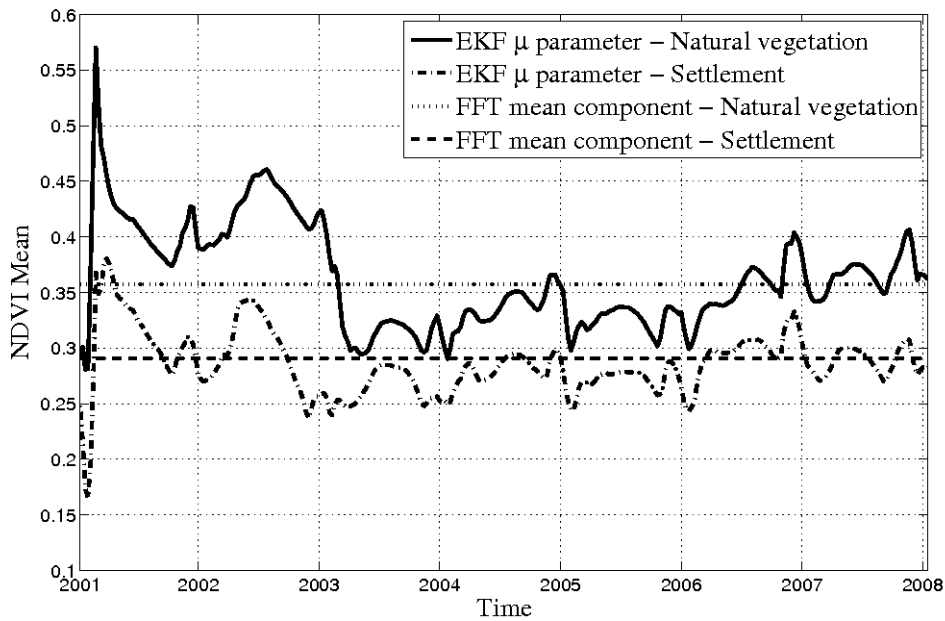
FIGURE 6.4: Comparing the EKF derived μ parameter with the FFT mean component for natural vegetation and settlement for region A.

component for two typical NDVI time-series belonging to each of the two classes in region A.

The μ sequence for the settlement and natural vegetation time-series clearly vary in similarity (Figure 6.4). This is to be expected as land-cover classes tend to be more similar during certain seasons than others. This characteristic was exploited by only considering the maximum distance between each pair of parameter sequences.

In essence, both approaches takes as input two NDVI time-series and outputs two distance metrics, D_μ and D_α, which is then subsequently used to quantify the similarity between these two NDVI time-series. In order to determine which of these methods produce the best measure of similarity, the joint distribution of D_μ and D_α can be calculated using same-class NDVI time-series examples ($p(D_\mu, D_\alpha|s)$) and then compared to the corresponding distribution using different-class NDVI time-series examples ($p(D_\mu, D_\alpha|d)$). By integrating the relevant densities over the overlapping areas of these distributions, the Bayes' error can be calculated and used to determine the performance of each method. The underlying idea is that the lower the Bayes' error, the more "unique" the distributions and consequently, the better the class separability. $p(D_\mu, D_\alpha|s)$ was estimated by comparing the NDVI time-series of each pixel in the natural vegetation class with each pixel in the natural vegetation class, as well as each pixel in the settlement class with each pixel in the settlement class, calculating

D_μ and D_α for each instance. Similarly, $p(D_\mu, D_\alpha|d)$ was estimated by comparing the NDVI time-series of each pixel in the natural vegetation class with each of the pixels in the settlement class and calculating D_μ and D_α for each instance. The distributions $p(D_\mu, D_\alpha|s)$ and $p(D_\mu, D_\alpha|d)$ where estimated by means of the Parzen-Rosenblatt window method using Gaussian kernels [105, 106].

For the EKF method, the initial state parameters as well as the observation and process noise estimates were determined off-line, based on known training data from the study areas. The training data were a random selection of 5% of the total number of pixels per region. The initial state parameters were calculated using the FFT mean and annual components of the training data as

$$\mu_1 = \sum_{i=1}^{Z} \frac{\mathbf{Y}_0^i}{Z}, \tag{6.1}$$

$$\alpha_1 = \sum_{i=1}^{Z} \frac{2\|\mathbf{Y}_7^i\|}{Z}, \tag{6.2}$$

$$\phi_1 = \sum_{i=1}^{Z} \frac{\angle \mathbf{Y}_7^i}{Z}. \tag{6.3}$$

Where Z is the total number of training time-series and $\mathbf{Y}_n^i$ is the n'th FFT component of time-series i. The observation noise was determined as

$$\sigma_v = \sum_{i=1}^{Z} \frac{\text{std}(\mathbf{e}_i)}{Z} \tag{6.4}$$

$$\mathbf{e}_i = \|\hat{\mathbf{y}}_i - \mathbf{y}_i\|. \tag{6.5}$$

Here σ_v is the estimated standard deviation of the observation noise, $\text{std}(\mathbf{e}_i)$ is the standard deviation of a vector containing the difference between the original time-series $\mathbf{y}_i$ and a filtered version $\hat{\mathbf{y}}_i$ calculated as

$$\hat{\mathbf{y}}_i = \mathbf{F}_N^{-1} \hat{\mathbf{Y}}^i. \tag{6.6}$$

$\hat{\mathbf{Y}}^i$ is defined as

$$\widehat{Y}^i(k) = \begin{cases} Y^i(k), & k = \{0, 7\} \\ 0, & 1 \leq k \leq 6 \\ 0, & 8 \leq k \leq N \end{cases}, \tag{6.7}$$

TABLE 6.1: Initial EKF state parameter values.

Region	μ_1	α_1	ϕ_1
A	0.3008	0.0835	0.2700
B	0.3447	0.1185	0.1708

TABLE 6.2: EKF observation and process noise values.

Region	σ_v	σ_μ	σ_α	σ_ϕ
A	3.8×10^{-2}	8×10^{-5}	8×10^{-5}	1.5×10^{-2}
B	4.4×10^{-2}	9×10^{-5}	9×10^{-5}	1.7×10^{-2}

and $\mathbf{F}_N^{-1}$ denotes the inverse DFT operation. $\hat{\mathbf{Y}}^i$ is thus a copy of $\mathbf{Y}^i$ but with only the mean and seasonal FFT components. All other components were set to zero.

The initial state parameters as well as the observation and process noise standard deviation for region A and B is shown in Table 6.1 and 6.2 respectively. The values of μ_1, α_1 and ϕ_1 in Table 6.1 were calculated using equations (6.1), (6.2) and (6.3) respectively. In Table 6.2, the observation noise variance σ_v was calculated using equations (6.4) and (6.5) while the process noise variance σ_μ, σ_α and σ_ϕ were estimated by maximizing the class separability on the training data for each region. This was done by determining the parameter distributions of each of the classes using the training data, and varying the ratio between σ_v and each of the process noise components. Using the maximum distance between distributions as criterion and a non-linear optimizer, the corresponding process noise parameters were determined.

Once determined, the parameters were kept fixed for all numerical results relating to the specific region. Figure 6.5 shows the joint distribution of D_μ and D_α using the FFT method (A) and EKF method (B) respectively. Here, $p(D_\mu, D_\alpha | s_f)$ is the distribution of D_μ and D_α calculated using the FFT method and using same class NDVI examples, $p(D_\mu, D_\alpha | d_f)$ is the distribution of D_μ and D_α calculated using the FFT method and using different class NDVI examples, $p(D_\mu, D_\alpha | s_k)$ is the distribution of D_μ and D_α calculated using the EKF method and using same class NDVI examples and $p(D_\mu, D_\alpha | d_k)$ is the distribution of D_μ and D_α calculated using the EKF method and using different
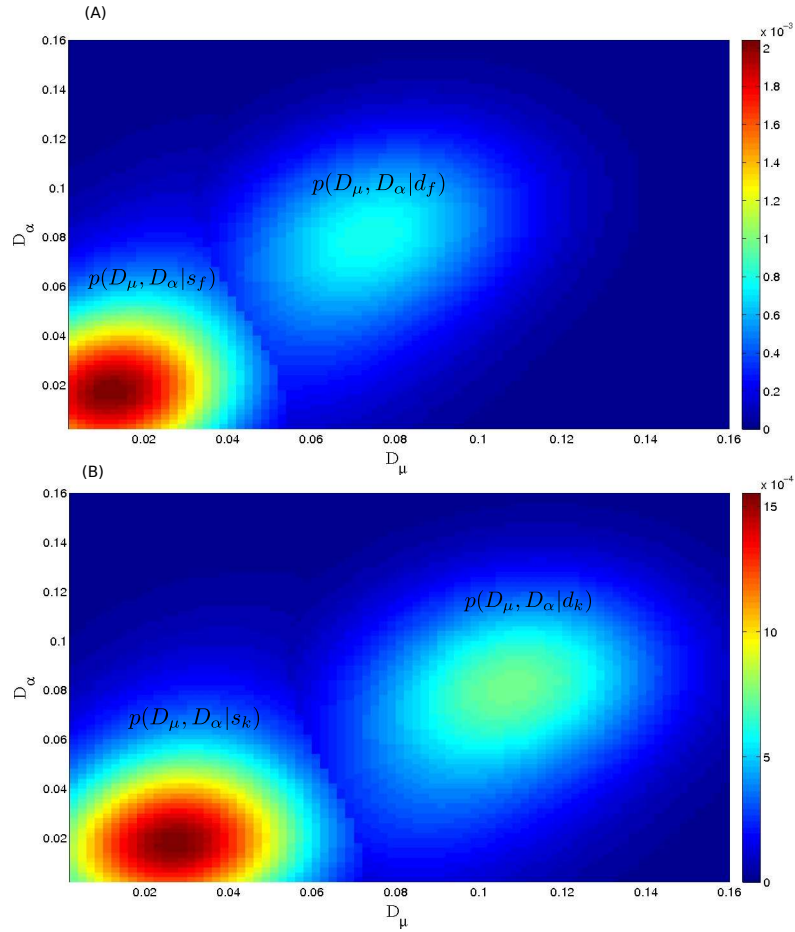
FIGURE 6.5: Joint distribution of D_μ and D_α using the FFT method (A) and EKF method (B) where $p(D_\mu, D_\alpha|s_f)$ is the distribution of D_μ and D_α calculated using the FFT method and using same class NDVI examples, $p(D_\mu, D_\alpha|d_f)$ is the distribution of D_μ and D_α calculated using the FFT method and using different class NDVI examples, $p(D_\mu, D_\alpha|s_k)$ is the distribution of D_μ and D_α calculated using the EKF method and using same class NDVI examples and $p(D_\mu, D_\alpha|d_k)$ is the distribution of D_μ and D_α calculated using the EKF method and using different class NDVI examples.

class NDVI examples. Table 6.3 gives the Bayesian decision error for both the FFT and EKF methods as well as the standard deviation of the error. The standard deviation was computed by using a random subset of 90% of the time-series to estimate the distributions $p(D_\mu, D_\alpha|s)$ and $p(D_\mu, D_\alpha|d)$ to infer the Bayes' error, and then repeating the experiment 10 times.

Consistent with most EKF implementations, the tracking of state parameters is not instantaneous and does require a certain number of observations. As this period is unknown, an initial number of state parameter values need to be excluded when calculating D_α and D_μ. The average square difference between the EKF derived μ parameter and the FFT mean component is shown in figure 6.6, it can be seen that the variation seems to stabilize within the first two years which relates to approximately 100 samples.
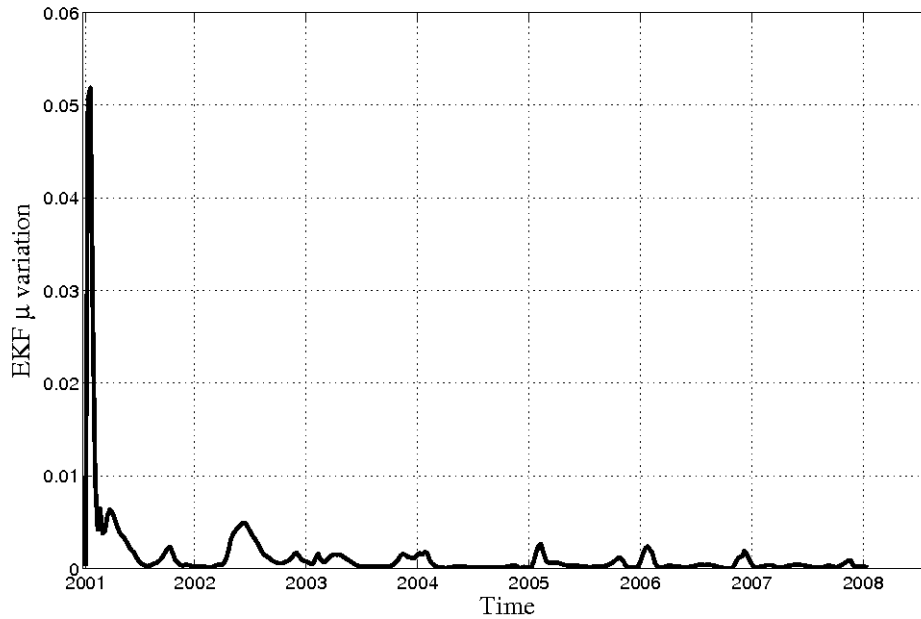
FIGURE 6.6: Average square difference between the EKF derived μ parameter and the FFT mean component for all settlement pixels in Region A.

It can be seen from Table 6.3 that the Bayesian decision error in region A (P_e^{EKF}) using the EKF was reduced by nearly 5% over the FFT method (P_e^{FFT}). In region B the Bayes' error of the EKF method was reduced by 2.63% over the FFT method. The standard deviation of the error probability was also reduced using the EKF method for both regions. Thus, overall it may be concluded that the EKF formulation has a reduced probability of error which implies that the EKF formulation offers improved separability of land-cover classes for the study areas A and B. The phase parameter ϕ was found to provide negligible additional separability (less than 0.01%) in the classes and was consequently disregarded.

As discussed in section 4.5, a sliding window alternative was proposed to extend on the FFT method presented in [56]. The mean and amplitude could be extracted by considering the relevant FFT components of a windowed FFT iterating through the time-series with the value of D_μ and D_α being calculated in an identical manner as was proposed for the EKF method (see section 4.5). The Bayes' error for the EKF, FFT and sliding window (SW) FFT method together with the corresponding variance of each of these methods are shown in figure 6.7 . The window size of the SW FFT method was varied between one and five years, denoted as SW FFT 1 to SW FFT 5 (figure 6.7).

Table 6.3: Bayes' error of the FFT and EKF method for region A and B. Percentage in parentheses indicates the standard deviation of the error.

Region	P_e^{FFT}	P_e^{EKF}
A	9.33% (1.95%)	4.34% (0.77%)
B	5.85% (1.60%)	3.22% (1.24%)

The overall improved separability of natural vegetation and settlement land-cover types using the EKF based on a triply modulated cosine function model over FFT and sliding window FFT is evident for both regions A and B. In an effort to improve the results, a sum of sinusoids model was also considered but preliminary results showed a negligible performance increase with a significant increase in the complexity as more parameters needed to be estimated. This corresponds to results shown in [56], where no significant added separability was achieved when considering more sinusoidal components other than the annual component.

In conclusion, the initialization procedure used to determine the initial EKF parameters as shown in section 6.2.2 was found to work well for each region. By using an initial training set and keeping the EKF initialization parameters constant for each region, the EKF is effectively adaptable for each region and requires minimal manual parameter selection. It was also found that the sliding window FFT method did improve on the standard FFT method when the correct window size was selected. The optimal window size for region A was 2 years whereas the optimal window size for region B was 1 year (figure 6.7). The EKF method had a lower percentage error compared to the sliding window FFT, regardless of the window size.
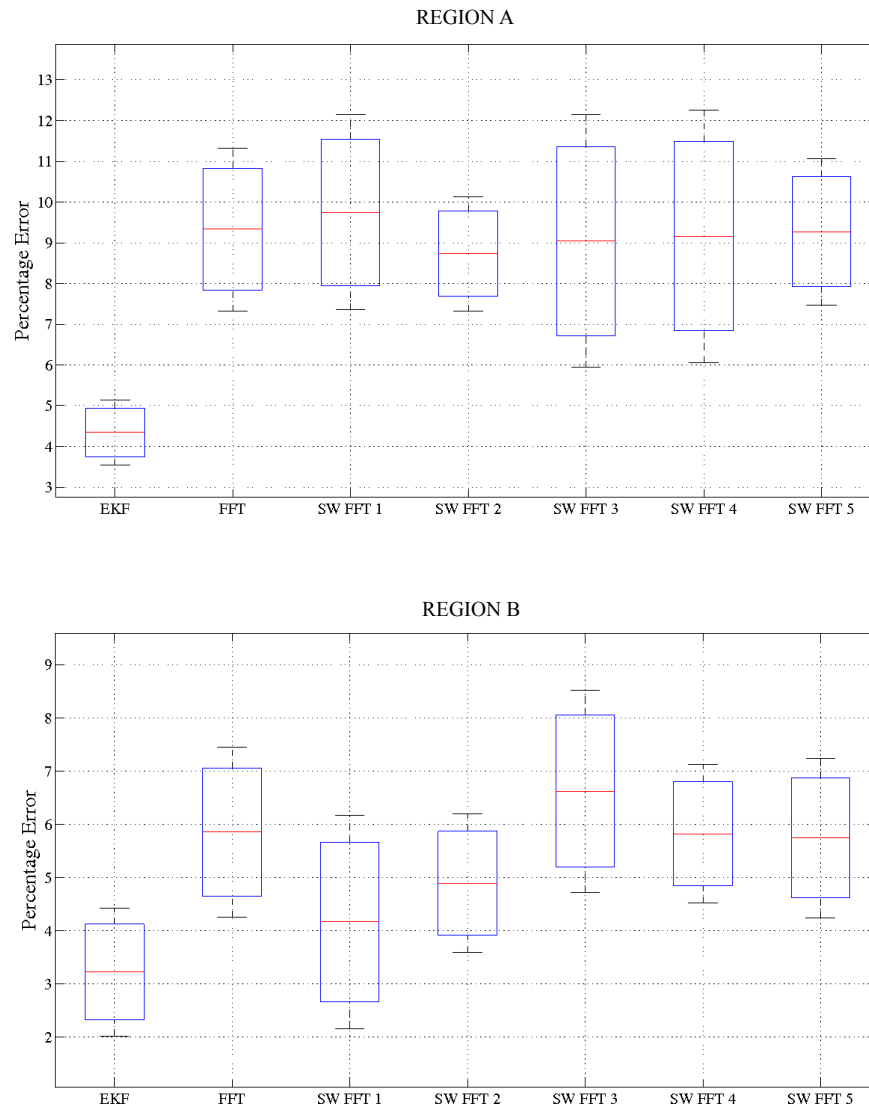
REGION A

REGION B

FIGURE 6.7: The Bayes' error and variance for the EKF, FFT and SW FFT method for region A and B. The window size of the SW FFT method was varied between one and five years.

6.3   DETECTING LAND-COVER CHANGE IN THE LIMPOPO PROVINCE OF SOUTH AFRICA

The Limpopo province is located in the northern region of South Africa. Figure 6.8 shows the location of the province. In this region, large families typically live under low-density conditions as opposed to high density squatter communities that live on the urban fringe in southern regions [7]. The province has a history of isolation from major urban and industrial centers. When compared to the rest of the country, people in this province are more reliant on subsistence production. Limpopo is one of the poorest provinces with more than 70% of people living under the poverty line [107]. The predominant land-cover type in the province is natural vegetation with the land use being mostly informal [107].
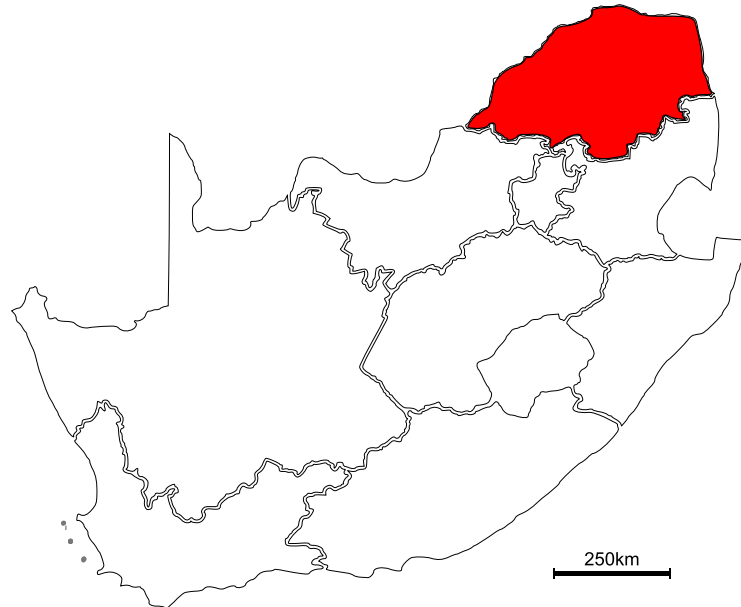
FIGURE 6.8: Location of the Limpopo province in South Africa.

The study area covers an approximate 25 000 km^2 having an upper left coordinate of ($23°20'12.09''$S ; $28°35'25.18''$E) and a lower right coordinate of ($25°00'14.59''$S ; $30°06'58.30''$E).

A total of 1 497 examples of natural vegetation, 1 735 examples of settlement and 117 examples of real change 500 m MODIS pixels were identified within the study area. Landsat and SPOT high resolution data were used to identify the aforementioned pixels as described in section 6.1.

6.3.1 Evaluation of the EKF change detection method in Limpopo

6.3.1.1 Off-line optimization of the EKF method in Limpopo

The simulated change dataset was generated using the methodology proposed in section 5.2.2. Roughly half (750 pixels) of the natural vegetation dataset were used to generate the simulated dataset. Each of these pixels were blended with a settlement pixel as described in section 5.2.2. The value of δ^* (as described in section 5.2.2) is shown for 6, 12 and 24 month blending periods in tables 6.4, 6.5 and 6.6 respectively. It is clear that the value of δ^* varies between 1.68 (when only the center pixel changing over a six-month period) and 1.37 (when all 9 pixels are changing over a 24-month period).

Table 6.4: Land-cover change detection accuracy, false alarm rate and optimal threshold (δ^*) for a range of pixels having changed in the 3×3 pixel grid using the EKF change detection method in Limpopo. The simulated change had a 6-month blending period and the value in parentheses indicates the standard deviation.

Number of pixels changed in 3×3 grid	Detection accuracy	False alarm rate	δ^*
1	91.79% (0.91%)	7.92% (0.67%)	1.68 (0.03)
2	92.90% (0.84%)	8.48% (0.62%)	1.65 (0.03)
3	92.59% (0.62%)	8.61% (0.60%)	1.66 (0.02)
4	92.63% (0.58%)	9.19% (0.93%)	1.63 (0.02)
5	92.70% (0.71%)	10.03% (1.21%)	1.59 (0.03)
6	93.11% (1.04%)	11.21% (0.60%)	1.56 (0.01)
7	92.73% (1.06%)	12.87% (0.93%)	1.52 (0.01)
8	90.88% (0.83%)	14.78% (0.73%)	1.47 (0.01)
9	90.42% (0.93%)	17.83% (1.01%)	1.42 (0.01)

The corresponding false alarm rate varies between 7.92% and 22.13% respectively. It follows that the operator needs to choose the maximum desirable false alarm rate in the aforementioned false alarm rate range. For this application, that maximum false alarm rate was chosen to be 13%. Substituting these values in equation 5.11:

$$\widehat{\delta} = \delta^* \;\; \text{where} \int_{\delta=\delta^*}^{\delta=\infty} p(\delta|\overline{C}) = 13\% \;\; \delta^* \in [1.36, 1.68], \tag{6.8}$$

$\widehat{\delta}$ was calculated as 1.5 and was used to determine change in the operational phase, as will be discussed in the following section.

6.3.1.2 Real change detection performance of the EKF method in Limpopo

Substituting the value of $\widehat{\delta}$ yields,

$$\text{Change} = \begin{cases} \text{true} & \text{if } \delta \geq 1.5 \\ \text{false} & \text{if } \delta < 1.5. \end{cases}$$

The change detection accuracy using the threshold of 1.5 was 89% using the 117 examples of real change in the study area. The false alarm rate was 13%.

Table 6.5: Land-cover change detection accuracy, false alarm rate and optimal threshold (δ^*) for a range of pixels having changed in the 3×3 pixel grid using the EKF change detection method in Limpopo. The simulated change had a 12-month blending period and the value in parentheses indicates the standard deviation.

Number of pixels changed in 3×3 grid	Detection accuracy	False alarm rate	δ^*
1	91.22% (0.96%)	7.92% (1.09%)	1.68 (0.04)
2	91.97% (0.84%)	8.24% (0.67%)	1.66 (0.02)
3	92.56% (0.65%)	8.64% (0.84%)	1.64 (0.03)
4	92.46% (1.16%)	9.27% (1.15%)	1.62 (0.02)
5	92.65% (0.95%)	10.38% (0.93%)	1.59 (0.02)
6	92.69% (0.60%)	11.53% (1.03%)	1.55 (0.01)
7	91.65% (1.25%)	13.06% (0.87%)	1.50 (0.02)
8	89.77% (1.11%)	15.25% (0.89%)	1.46 (0.01)
9	89.65% (0.91%)	18.83% (0.98%)	1.40 (0.01)

Table 6.6: Land-cover change detection accuracy, false alarm rate and optimal threshold (δ^*) for a range of pixels having changed in the 3×3 pixel grid using the EKF change detection method in Limpopo. The simulated change had a 24-month blending period and the value in parentheses indicates the standard deviation.

Number of pixels changed in 3×3 grid	Change simulated	No Change simulated	δ^*
1	91.46% (0.74%)	9.25% (0.79%)	1.63 (0.02)
2	91.54% (1.20%)	9.33% (0.86%)	1.63 (0.01)
3	91.53% (0.65%)	10.25% (1.18%)	1.61 (0.02)
4	92.12% (0.66%)	11.10% (0.53%)	1.58 (0.02)
5	92.34% (0.86%)	11.52% (1.14%)	1.54 (0.01)
6	92.47% (0.58%)	13.69% (1.18%)	1.50 (0.01)
7	90.63% (0.82%)	14.93% (1.37%)	1.48 (0.01)
8	87.98% (0.49%)	17.53% (0.98%)	1.43 (0.01)
9	87.06% (1.24%)	22.13% (0.61%)	1.37 (0.01)

Table 6.7: Confusion Matrix, overall accuracy (O_A) and optimal threshold (δ^*) showing the best land-cover change detection performance during the ACF method's off-line optimization phase using MODIS band 4 *(550 nm)* with a lag of 104 days. Value in parentheses indicates the standard deviation.

	Simulated change (n=750)	No Change (n=1616)	δ^*	O_A
Change Detected	78.16% (1.5%)	12.25% (1.4%)	0.13 (0.01)	82.95% (1.4%)
No Change Detected	21.84% (1.5%)	87.75% (1.4%)		

6.3.2 Evaluation of the temporal ACF change detection method in Limpopo

6.3.2.1 Off-line optimization of the ACF method in Limpopo

As described in section 5.3.2, a subset of the no-change dataset, consisting of vegetation and settlement pixels were used in the off-line optimization phase. Of the available 1 497 examples of natural vegetation and 1 735 settlement pixels, 750 simulated change pixels were generated by linearly blending a time-series of a pixel covered by natural vegetation with that of a settlement pixel time-series (Section 5.3.2). The resulting simulated change database had a uniformly spread change date between 2001/01 and 2008/01. The blending period was found not to influence the method's performance [108], and a representative blending period of six months was chosen. From the total of 3 232 no-change pixels, a random selection of 1 616 pixels were used during the off-line optimization phase with the remainder (1 616 pixels) being used to infer the false alarm rate performance during the real change detection phase.

The overall accuracy (O_A) as calculated in (5.19) was calculated for each band $b \in \{1, 2, ..., 8\}$ and lag $\tau \in \{1, 2, ..., 46\}$ using the no-change and change dataset described above is shown in figure 6.9. It was found that the highest overall detection accuracy was obtained by using the change index $\delta_\tau^b = \delta_{13}^4 = R^4(13)$. Because the time-series has an observation of 8 days, the τ value of 13 corresponds to 104 days. The value of δ_{13}^{4*} was found to be 0.13. Table 6.7 summarizes the performance of the method when using the aforementioned parameters.

6.3.2.2 Real change detection performance of the ACF method in Limpopo

After the band, lag and optimal threshold selection was completed, the performance of the proposed method was validated using the no-change and real change datasets. A change or no-change decision for each pixel was obtained by evaluating
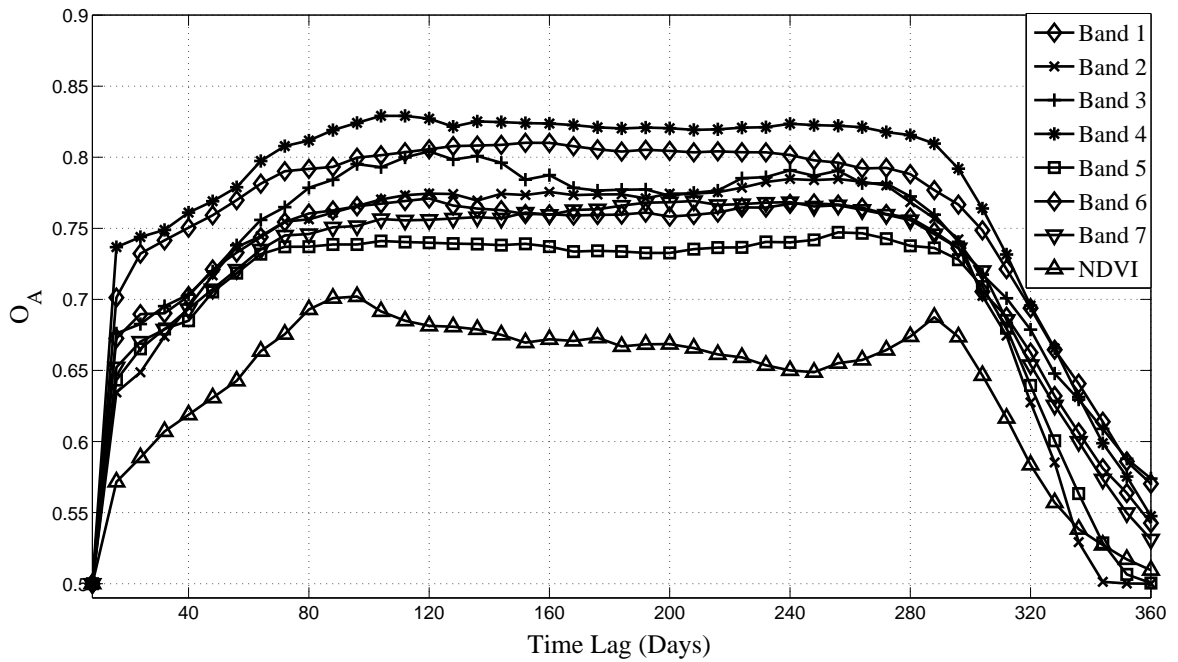
FIGURE 6.9: Overall accuracy of the ACF method computed for a range of band and lag combinations using a no-change and simulated change dataset for the Limpopo province.

$$\text{Change} = \begin{cases} \text{true} & \text{if } R^b(\tau) \geq 0.13 \\ \text{false} & \text{if } R^b(\tau) < 0.13. \end{cases}$$

Table 6.8 summarizes the performance of the method using the parameters obtained during the off-line optimization phase.

Table 6.8: Confusion Matrix, overall accuracy (O_A) and threshold (δ) for the case of real change detection using the MODIS band 4 *(550 nm)* with a lag of 104 days as determined during the ACF method's off-line optimization phase. Value in parentheses indicates the standard deviation.

	Real change (n=117)	No Change (n=1616)	δ	O_A
Change Detected	81.20% (2.7%)	12.00% (1.1%)	0.13 (0.01)	84.60% (2%)
No Change Detected	18.80% (2.7%)	88.00% (1.1%)		

Table 6.9: Confusion matrix of the NDVI differencing method using a fixed and optimal threshold for the Limpopo province. Value in parentheses indicates the standard deviation.

	Real change (n=117)	No Change (n=1616)	z	O_A
Fixed false alarm rate			2.1	77.79% (1.8%)
Change Detected	69.00% (3.7%)	13.00% (1.0%)		
No Change Detected	31.00% (3.7%)	87.00% (1.0%)		
Optimal Threshold			1.6 (0.2)	79.21% (1.3%)
Change Detected	83.76% (4.7%)	25.34% (4.1%)		
No Change Detected	16.24% (4.7%)	15.40% (4.1%)		

6.3.3   Evaluation of the NDVI differencing method in Limpopo

Using the methodology given in section 5.4, the NDVI differencing change detection method was applied in the Limpopo province, Table 6.9 shows the performance of the method using an optimal threshold as well as the threshold corresponding to a constant false alarm rate of 13%. To get an indication of the NDVI method's performance as a function of z, the false alarm rate and change detection accuracy was calculated for a series of z values ranging from 1 to 3.5 (figure 6.10). The optimal threshold (z^*) and the threshold corresponding to a false alarm rate of 13% (z) is indicated on the false alarm rate curve.

6.4   DETECTING LAND-COVER CHANGE IN THE GAUTENG PROVINCE OF SOUTH AFRICA

The Gauteng province is located in northern South Africa, because of a high level of urbanization it has seen significant human settlement expansion during the 2001 and 2008 period. A total area of approximately 17 000 km^2 was considered being centered around $26°07'29.62''$S, $28°05'40.40''$E. Figure 6.11 shows the location of the Gauteng province in South Africa. Gauteng is the smallest province in South Africa, occupying a land area of only 1.4% of the land area of the country, but it is highly urbanized as it contains two of the largest cities in South Africa, Johannesburg and Pretoria.

A total of 592 examples of natural vegetation, 372 examples of settlement and 181 examples of real change 500 m MODIS pixels were identified within the study area. Landsat and SPOT high resolution
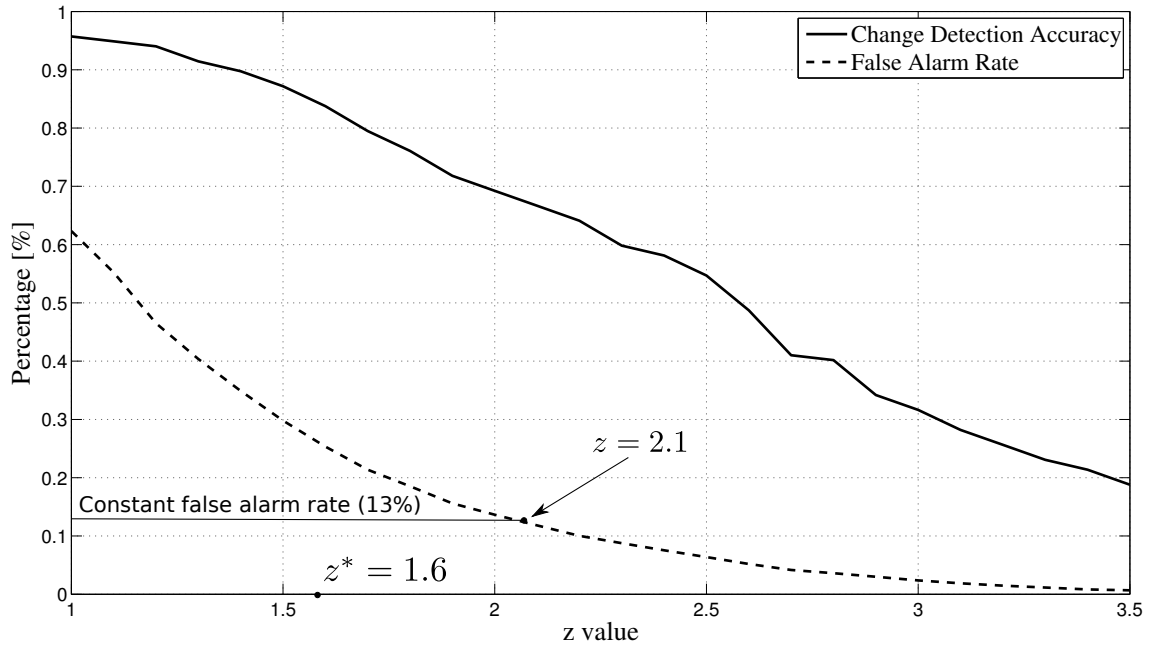
FIGURE 6.10: NDVI differencing method's change detection accuracy and false alarm rate for a range of z values in Limpopo.

data were used to identify the aforementioned pixels as described in section 6.1.

6.4.1 Evaluation of the EKF change detection method in Gauteng

6.4.1.1 Off-line optimization of the EKF method in Gauteng

The simulated change dataset was also generated using the methodology proposed in section 5.2.2. In this case, 296 pixels in the natural vegetation dataset were used to generate the simulated dataset. The value of δ^* (as described in section 5.2.2) is shown for 6, 12 and 24 month simulated blending periods in tables 6.10, 6.11 and 6.12 respectively. The value of δ^* varied between 2.5 and 1.91 with a corresponding false alarm rate being between 3.62% and 16.05% respectively. As in the previous study area, a maximum false alarm rate was chosen to be 13%. Substituting these values in Equation 5.11

$$\widehat{\delta} = \delta^* \ \text{ where } \int_{\delta=\delta^*}^{\delta=\infty} p(\delta|\overline{C}) = 13\% \ \ \delta^* \in [1.91, 2.5], \tag{6.9}$$

$\widehat{\delta}$ was calculated as 1.975.

Table 6.10: Land-cover change detection accuracy, false alarm rate and optimal threshold (δ^*) for a range of pixels having changed in the 3×3 pixel grid using the EKF change detection method in Gauteng. The simulated change had a 6-month blending period and the value in parentheses indicates the standard deviation.

Number of pixels changed in 3×3 grid	Detection accuracy	False alarm rate	δ^*
1	99.29% (0.40%)	3.33% (0.59%)	2.49 (0.06)
2	99.23% (0.34%)	3.15% (0.56%)	2.49 (0.04)
3	99.44% (0.43%)	3.63% (0.60%)	2.45 (0.04)
4	98.86% (0.32%)	4.17% (0.73%)	2.44 (0.03)
5	98.09% (0.67%)	4.88% (1.03%)	2.36 (0.05)
6	98.26% (0.97%)	7.26% (1.03%)	2.22 (0.03)
7	98.52% (0.37%)	8.69% (0.80%)	2.14 (0.02)
8	97.11% (0.75%)	9.32% (1.45%)	2.09 (0.02)
9	95.14% (0.84%)	11.39% (1.07%)	2.02 (0.01)

Table 6.11: Land-cover change detection accuracy, false alarm rate and optimal threshold (δ^*) for a range of pixels having changed in the 3×3 pixel grid using the EKF change detection method in Gauteng. The simulated change had a 12-month blending period and the value in parentheses indicates the standard deviation.

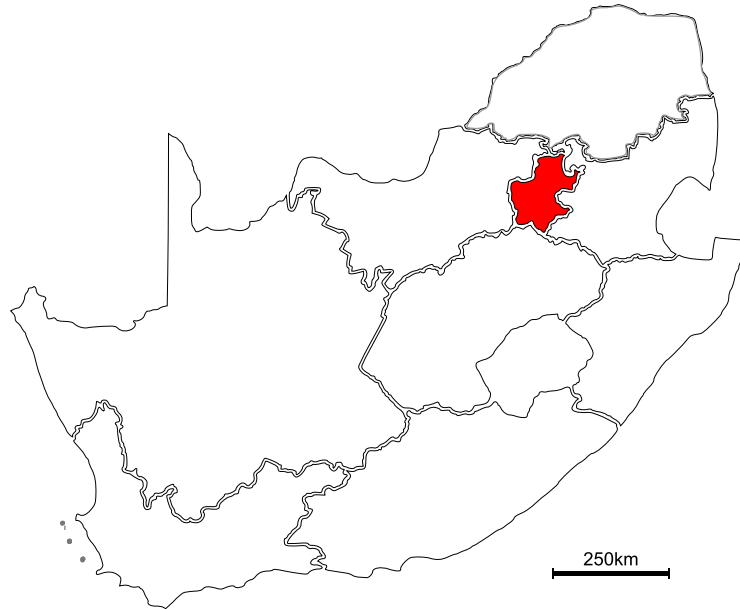| Number of pixels changed in 3×3 grid	Detection accuracy	False alarm rate	δ^*
1	99.44% (0.38%)	3.62% (0.79%)	2.50 (0.04)
2	99.29% (0.40%)	3.76% (0.82%)	2.42 (0.05)
3	99.29% (0.41%)	4.24% (0.39%)	2.38 (0.04)
4	98.99% (0.49%)	4.45% (0.73%)	2.37 (0.05)
5	98.29% (0.65%)	5.98% (0.73%)	2.28 (0.04)
6	98.44% (0.63%)	8.18% (0.83%)	2.16 (0.04)
7	98.24% (0.49%)	8.89% (0.66%)	2.10 (0.02)
8	97.37% (0.75%)	10.28% (0.85%)	2.05 (0.03)
9	94.58% (0.94%)	12.79% (1.07%)	1.97 (0.02)

FIGURE 6.11: Location of the Gauteng province in South Africa.

6.4.1.2   Real change detection performance of the EKF method in Gauteng

Substituting the value of $\widehat{\delta}$ yields,

$$\text{Change} = \begin{cases} \text{true} & \text{if } \delta \geq 1.97 \\ \text{false} & \text{if } \delta < 1.97. \end{cases}$$

The change detection accuracy using the threshold of 1.97 was 75% using the 181 examples of real change in the study area. The false alarm rate was 12.75%.

6.4.2   Evaluation of the temporal ACF change detection method in Gauteng

6.4.2.1   Off-line optimization of the ACF method in Gauteng

Of the available 592 examples of natural vegetation and 372 settlement pixels, 592 simulated change pixels were generated. From the total of 964 no-change pixels, a random selection of 482 pixels were used during the off-line optimization phase with the remainder (482 pixels) being used to infer the false alarm rate performance during the real change detection phase.

Table 6.12: Land-cover change detection accuracy, false alarm rate and optimal threshold (δ^*) for a range of pixels having changed in the 3×3 pixel grid using the EKF change detection method in Gauteng. The simulated change had a 24-month blending period and the value in parentheses indicates the standard deviation.

Number of pixels changed in 3×3 grid	Detection accuracy	False alarm rate	δ^*
1	99.25% (0.48%)	4.50% (0.77%)	2.40 (0.04)
2	99.29% (0.35%)	4.78% (0.79%)	2.37 (0.05)
3	99.01% (0.56%)	5.28% (0.65%)	2.34 (0.04)
4	98.20% (0.82%)	5.82% (0.66%)	2.28 (0.04)
5	97.73% (0.64%)	8.51% (0.60%)	2.18 (0.03)
6	97.75% (1.09%)	9.53% (0.95%)	2.09 (0.02)
7	97.71% (0.88%)	10.53% (0.65%)	2.04 (0.03)
8	94.92% (1.55%)	12.37% (1.03%)	1.98 (0.01)
9	91.61% (0.70%)	16.05% (1.25%)	1.91 (0.02)

O_A was calculated for each band $b \in \{1, 2, ..., 8\}$ and lag $\tau \in \{1, 2, ..., 46\}$ using the aforementioned no-change and simulated change datasets (figure 6.12). It was found that the highest overall detection accuracy was obtained by using the change index $\delta_\tau^b = \delta_{12}^4 = R^4(12)$. The τ value of 12 corresponds to 96 days. The value of δ_{12}^{4*} was found to be 0.16. Table 6.13 summarizes the performance of the method when using the aforementioned parameters.

Table 6.13: Confusion Matrix, overall accuracy (O_A) and optimal threshold (δ^*) showing the best land-cover change detection performance during the ACF method's off-line optimization phase using MODIS band 4 *(550 nm)* with a lag of 96 days. Value in parentheses indicates the standard deviation.

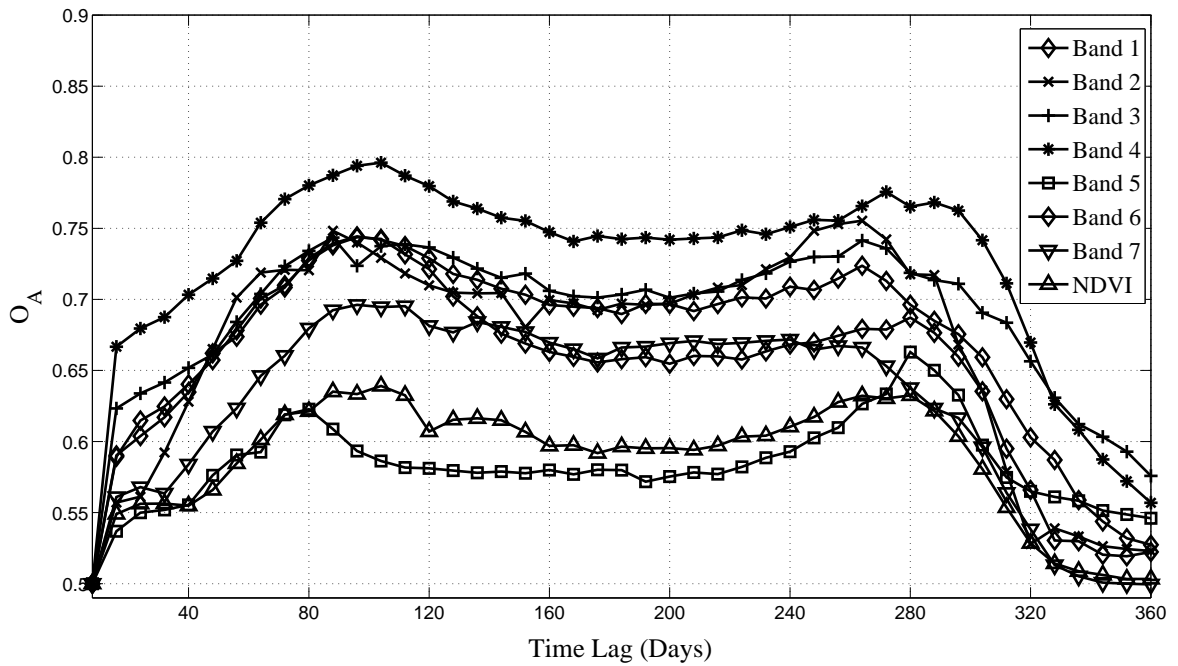|	Simulated change (n=592)	No Change (n=482)	δ^*	O_A
Change Detected	75.17%(4.0%)	14.73% (1.6%)	0.16 (0.01)	80.22% (2%)
No Change Detected	24.83% (4.0%)	85.27% (1.6%)		

FIGURE 6.12: Overall accuracy evaluated for a range of band and lag combinations using a no-change and simulated change dataset for the Gauteng province.

6.4.2.2 Real change detection performance of the ACF method in Gauteng

After the band, lag and optimal threshold selection was completed, the performance of the proposed method was validated using the no-change and real change datasets. A change or no-change decision for each pixel was obtained by evaluating

$$\text{Change} = \begin{cases} \text{true} & \text{if } R^b(\tau) \geq 0.16 \\ \text{false} & \text{if } R^b(\tau) < 0.16. \end{cases}$$

Table 6.14 summarizes the performance of the method using the parameters obtained during the off-line optimization phase.

6.4.3 Evaluation of the NDVI differencing method in Gauteng

Using the methodology given in section 5.4, the NDVI difference change detection method was used in the Gauteng province, Table 6.15 shows the performance of the method at the optimal threshold as well as the threshold corresponding to a constant false alarm rate of 13%. Figure 6.13 shows the false alarm rate and change detection accuracy as a function of the z value.

Table 6.14: Confusion Matrix, overall accuracy (O_A) and threshold (δ) for the case of real change detection using the MODIS band 4 *(550 nm)* with a lag of 96 days as determined during the ACF method's off-line optimization phase. Value in parentheses indicates the standard deviation.

	Real change (n=181)	No Change (n=482)	δ	O_A
Change Detected	92.27% (4.5%)	15.35% (1.9%)	0.16 (0.02)	88.46% (3%)
No Change Detected	7.73% (4.5%)	84.65% (1.9%)		

Table 6.15: Confusion matrix of the NDVI differencing method using a fixed and optimal threshold for the Gauteng province. Value in parentheses indicates the standard deviation.

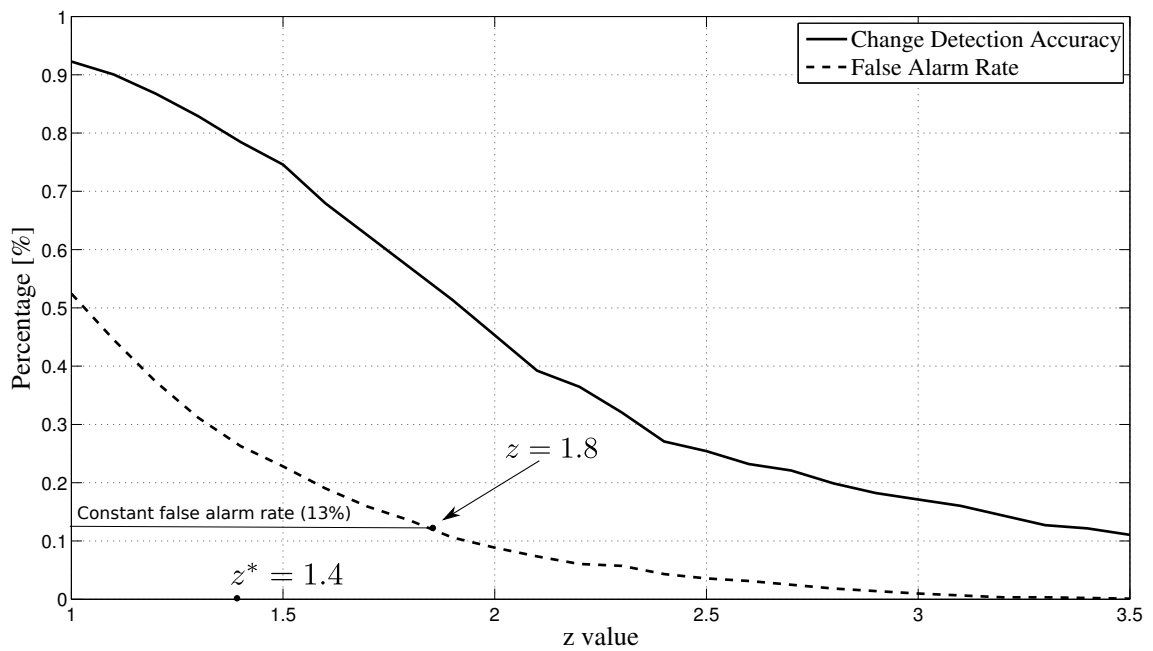|	Real change (n=181)	No Change (n=482)	z	O_A
Fixed false alarm rate				
Change Detected	56.91% (4.5%)	13.51% (1.0%)	1.8	71.70% (2.2%)
No Change Detected	43.09% (4.5%)	86.49% (1.0%)		
Optimal Threshold				
Change Detected	78.45% (4.2%)	26.27% (5.2%)	1.4 (0.11)	76.09% (1.7%)
No Change Detected	21.55%(4.2%)	73.73% (5.2%)		

FIGURE 6.13: NDVI differencing method's change detection accuracy and false alarm rate for a range of z values in Gauteng.

6.5   DISCUSSION OF THE CHANGE DETECTION METHODS

Table 6.16 gives a performance comparison of all the methods presented in this chapter. The threshold was selected so that the false alarm rate is within the 10% – 15% range to enable a fair comparison of all three methods. The following section will discuss the results obtained using each of these methods for the case of real change detection in greater detail.

6.5.1   Discussion of the EKF change detection method results

From Table 6.16 it is evident that the performance of the EKF method is acceptable in both provinces, achieving more than a 75% detection accuracy with the false alarm rate being less than 15% for each of the areas. The performance of the method is, however, better in the Limpopo region. The reason for this could be that the Limpopo province is mostly covered by natural vegetation which implies an inherent high correlation between pixels when considering a 3×3 pixel grid in a natural vegetation area. As was shown in tables 6.10, 6.11 and 6.12, the method performs best when fewer pixels in the 3×3 grid change, for example, 7.92% with only the center pixel changing versus 18.83% with all 9 pixels changing in the case of a 6-month simulated land cover change (Table 6.10). The conclusion can thus be drawn that the EKF method performs best in an environment where most of the pixels in

Table 6.16: Summary of real change detection results. Value in parentheses indicates the standard deviation.

Algorithm	No. of Real Change Pixels	% Change Correctly Detected	% False Alarms	Threshold
Limpopo Province				
EKF method	117	89% (2.8%)	13% (0.98%)	$\delta = 1.5$
ACF method	117	81% (4.5%)	12% (1.9%)	$\delta = 0.13$
NDVI Differencing method [17]	117	69% (3.7%)	13% (1.0%)	$z = 2.1$
Gauteng Province				
EKF method	181	75% (2.9%)	13% (0.9%)	$\delta = 1.97$
ACF method	181	92% (2.7%)	15% (1.1%)	$\delta = 0.16$
NDVI Differencing method [17]	181	57% (4.5%)	14% (1.3%)	$z = 1.8$

the 3×3 pixel grid are highly correlated. This was found to be the case in Limpopo as the province is mostly covered by natural vegetation. A typical 3×3 grid of pixels in Limpopo thus have a high probability of having the same land-cover type and consequently a high correlation when considering the EKF derived parameter sequences. In the case of Gauteng, being the smallest province with the highest population, the landscape is much more diverse. A typical 3×3 grid of pixels, which corresponds to an area of 2.25 km^2, has a much higher probability of having de-correlated pixels and subsequently, the method's performance in this area was compromised. To test this hypothesis, the standard deviation between the center pixel and neighboring pixels of a 3×3 pixel grid was calculated for all the pixels in the Limpopo and Gauteng study area. The underlying idea is that a low standard deviation would indicate that the grid area is more homogeneous than a pixel grid having a high standard deviation. A summer MODIS image over the Limpopo and Gauteng study area was used for the experiment. As expected, it was found that Gauteng had a 15% increase in the standard deviation relative to Limpopo. This finding was also supported when considering the bio-diversity in both study areas (Figure 6.15).

In an effort to determine the stability of the false alarm rate as a function of the region size, the EKF method was run blindly, i.e. without having any knowledge of the land cover type or usage, over a 70 km radius from the center of each study area in the Limpopo and Gauteng provinces (Figure

Limpopo Province
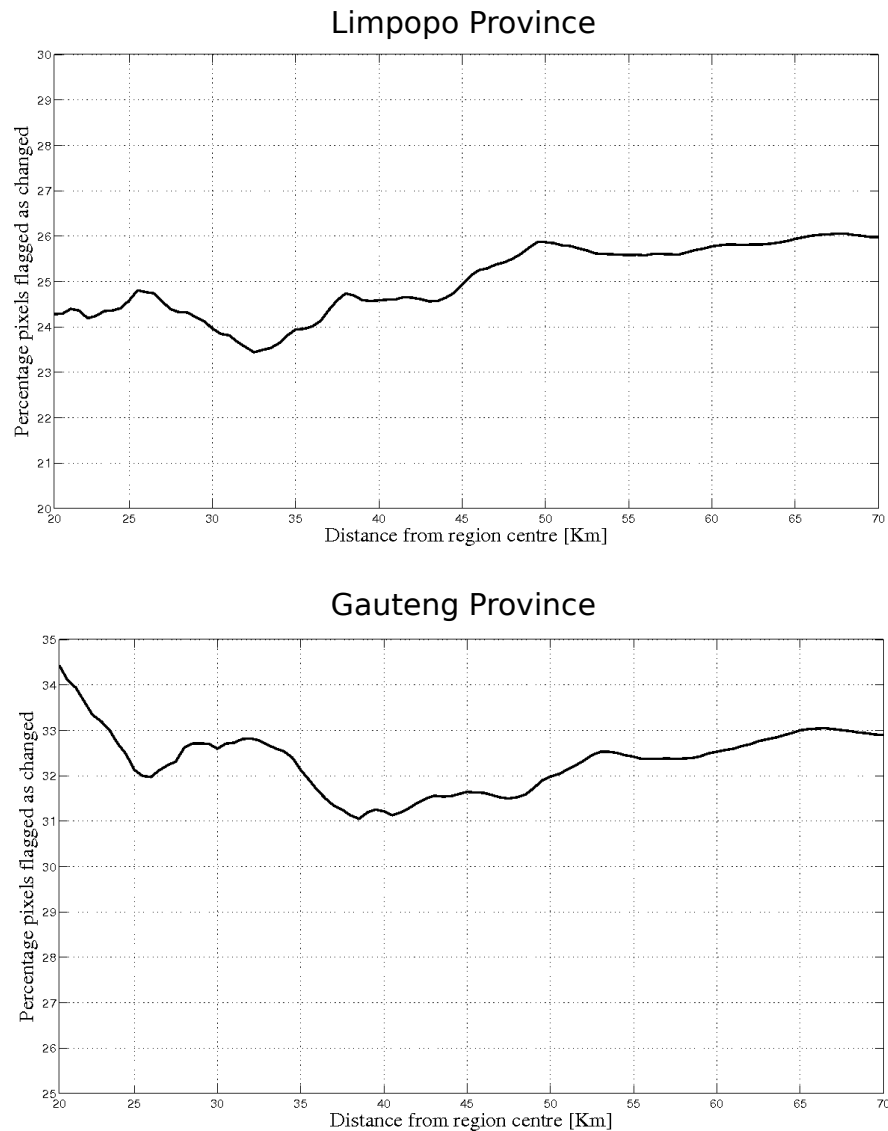

Gauteng Province

FIGURE 6.14: Percentage pixels flagged as changed as a function of the distance from the center of each region.

6.14). The rationale behind this experiment is that, with all other parameters being kept constant, there will be a dramatic change in the percentage pixels flagged as having changed if the threshold, which determines the false alarm rate, becomes invalid when increasing the radius of the operation. It is evident that the percentage pixels having changed does not vary significantly as a function of the distance from the region center, having a standard deviation of roughly 1% for both the Limpopo and Gauteng province. The 70 km radius was postulated to be representative when considering the bio-regions found in South Africa which are typically less than 140 km in diameter (Figure 6.15). Bio-regions are characteristic flora, fauna, and environmental conditions and as such would have to be taken into consideration when determining the threshold for operational use.
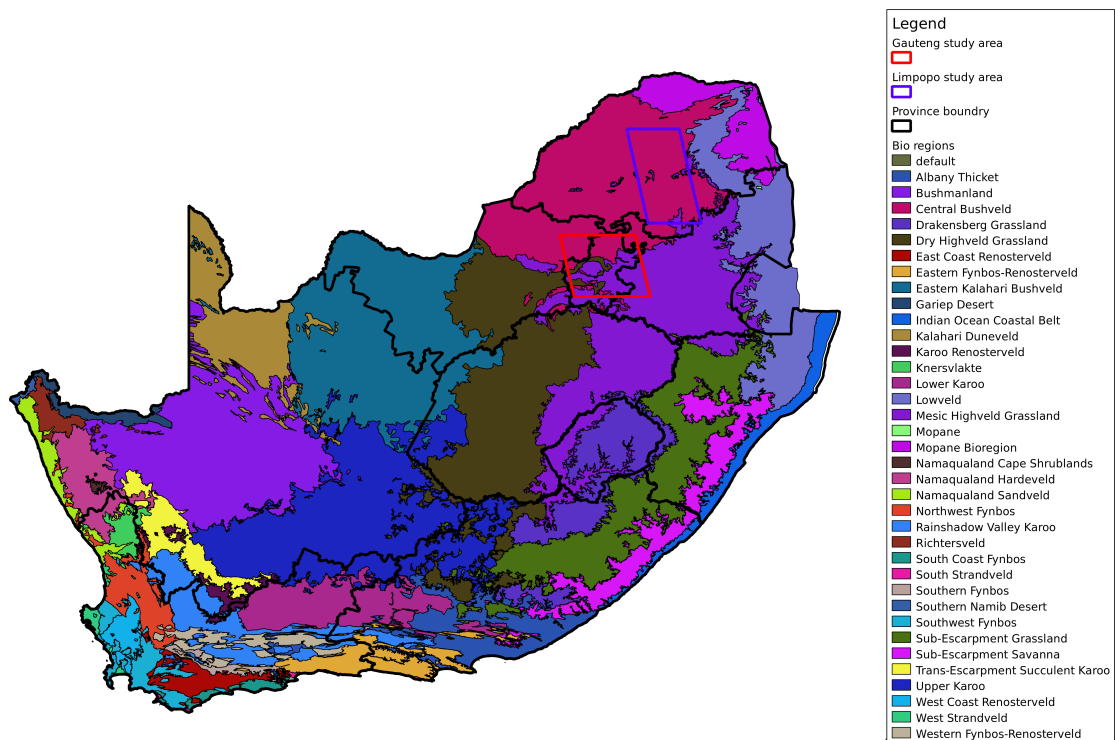
FIGURE 6.15: Location of the Gauteng and Limpopo study areas as well as the bio-regions found in South Africa.

Another interesting point is that the number of pixels having been flagged as changed which ranged between 24% and 34%. The false alarm rate in the study area using the predetermined threshold was found to be less than 14% (Table 6.16) in both provinces which raises the question of the source of the remaining 10 to 20%. One obvious source of the additional pixels being flagged as change, other than the false alarms, are pixels that did in fact change from a natural vegetation to settlement land cover and were consequently detected as having changed. As this type of change is a relatively rare event in a regional landscape (typically 4% according to F. Schoeman *et al.* [67]), it is highly unlikely that this is the only source of the additional percentage difference. It is safe to assume that land cover change from natural vegetation to settlement in both provinces is not the only type of land cover change possibility which implies that the additional 6 to 16% of pixels flagged as changed could be because of a host of other changes which could include, for example, agriculture, mining, deforestation, etc. It is very probable that the EKF change detection method was sensitive to these types of changes as well which could have resulted in the higher than expected number of pixels flagged as having changed. There is also a strong possibility that the EKF method could be sensitive to other land cover types, for example, water. Sensitivity for various types of land cover changes is advantageous when using the method as a change alarm, this thesis only considered settlement expansion as an example but the
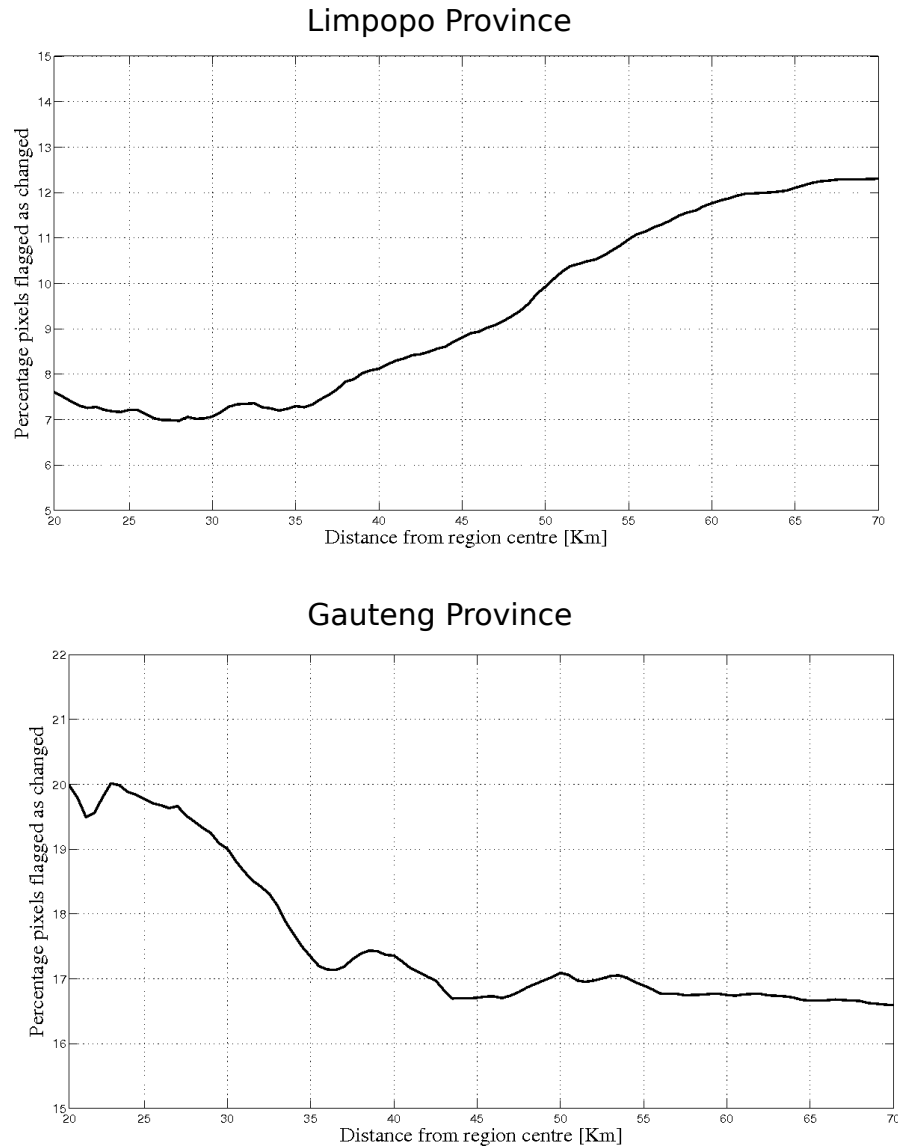
Limpopo Province

Gauteng Province

FIGURE 6.16: Percentage pixels flagged as changed using the ACF method as a function of the distance from the center of each region.

detection capability of the method to other land cover changes, for example deforestation is definitely a topic for further investigation (see section 7.2).

6.5.2   Discussion of the temporal ACF change detection method results

The ACF method performance is also acceptable, achieving more than an 80% detection accuracy with the false alarm being 15 % or lower for both provinces (Table 6.16). As opposed to the results obtained by the EKF change detection method, the performance of the temporal ACF change detection method is better for the Gauteng province than the Limpopo province. The performance of the false alarm rate of the temporal ACF change detection method in Limpopo is very similar for the

TABLE 6.17: O_A performance for different start of change dates.

Mean start of change	O_A
2001/06	70.67%
2002/06	83.57%
2003/06	85.33%
2004/06	85.43%
2005/06	84.92%
2006/06	81.74%
2007/06	76.66%

off-line optimization and operational phase being 12% and 12.25% respectively. The change detection accuracy for the corresponding areas were 78.16% and 81.20% respectively (Tables 6.7 and 6.8) which is also relatively similar. In the Gauteng province the false alarm rate for both the off-line optimization and operational phase was again very similar (14.73% and 15.35%), but the change detection accuracy was considerably different (75.17% and 92.27%). It might seem counterintuitive that the simulated change is more difficult to detect than real change examples in the Gauteng province, but this does make sense when considering the timing of the change. The mean start of change date of the real change dataset in Gauteng is 2004 with a standard deviation of two years. The simulated change date, on the other hand, was distributed uniformly over the entire date range of the time-series. Therefore, when the change occurs in the center of the time-series, the non-stationarity of the time-series will be at a maximum and will decrease as the change date moves towards the beginning or end of the time-series. The performance of the method for detecting simulated change is shown for different start years (Table 6.17). It is clear that the ACF change detection method is slightly compromised when change occurs in the first or last year with no significant decrease in the performance for the others years. Unfortunately, no change date information was available in the Limpopo province, only images at the start and end of the time-series. It is, however, very probable that the change date in Limpopo was distributed more uniformly over the study period, which resulted in the higher correlation between that simulated change and real change detection performance.

Combining multiple bands in this study did not significantly improve on the separability achieved using only band 4. This does not suggest that band 4 is the best for all types of land-cover change.

However, for our study area and land-cover change case, the ACF of the band 4 time-series showed the highest separability between the no-change and simulated change datasets. Multiple band combinations could also be used to improve the separability at the cost of increased computational complexity in cases where no single band gives adequate separability.

The stability of the false alarm rate for the ACF method was also evaluated as a function of the region size. Similar to the experiment shown in section 6.5.1, the ACF method was run blindly over a 70 km radius from the center of each study area in the Limpopo and Gauteng provinces (Figure 6.16). Although there was slightly more variation in the percentage pixels having changed compared to the EKF method, the ACF method does not vary significantly as a function of the distance from the region center, having a standard deviation of roughly 2% for both the Limpopo and Gauteng province. As with the corresponding experiment in the case of the EKF method, some interesting results where observed when considering the percentage of pixels flagged as having changed. The percentage of pixels flagged as having changed varied between 7 and 20%, which is much lower than the corresponding results obtained using the EKF method. The difference between the false alarm rate of less than 15% in both of the study regions (table 6.16) to that of the number of pixels flagged as having changed in the 'blind run' experiment is much smaller which indicates that the ACF method is potentially not so sensitive to other types of land cover changes using the parameters derived during the off-line optimization phase which made use of the simulated change and no-change datasets of natural vegetation and settlement land cover types.

6.5.3   Discussion of the NDVI differencing method

The NDVI differencing method, proposed in [17],was found not to be very successful, having a change detection accuracy of less than 70% in the false alarm region of 15% and less for both study areas (Table 6.16). A possible explanation for this is that because the NDVI differencing method assumes that the annual NDVI difference is distributed normally, the method could have difficulty in detecting land-cover change when the study area is heterogeneous and consequently compromises the normality assumption that is fundamental to this method. As expected, the method performs the poorest in the Gauteng province because of the land-cover diversity of the area (see figure 6.15). The method does perform better in the Limpopo province, but still has a change detection accuracy performance decrease of 20% when compared to the EKF change detection method at the same false alarm rate. The NDVI differencing method also reduces the eight day composited time-series over the seven-year period to an effective seven observations by only considering the total annual NDVI value for each year. This reduces the information available for change detection considerably. The threshold value

that corresponded with a false alarm rate in the region of 13% was between 1.8 and 2.1 (see figures 6.10 and 6.13) with the change detection accuracy being less than 70% in both cases. These results correspond well to those reported by Lunetta *et al.* for non-agricultural areas in the Albemarle-Pamlico estuary system (APES) located in North Carolina and Virginia in the United States. For their study, a threshold value of 2 resulted in a change detection accuracy of 68% with a false alarm rate of 15% [17].

6.6   CONCLUSION

In this chapter, the performance of three change detection methods was presented. Firstly, as a buildup to the EKF change detection framework, it was shown that that the separation between natural vegetation and settlement land-cover types can be improved over FFT separation by using an EKF (Section 6.2.2). After EKF separability between natural and settlement time-series data was determined, the method was adapted to the change detection case by formulating a change metric that is based on a comparison of the μ and α parameter sequences of a pixel to the EKF derived parameter sequences of its neighboring pixels. The EKF change detection method was used to detect new settlement developments in the Limpopo and Gauteng provinces of South Africa (section 6.3.1 and 6.4.1).

The second method that was proposed was the temporal ACF change detection method. The temporal ACF was used to exploit the non-stationarity of change pixels relative to no-change pixels by using the correlation coefficient of a pre-determined band and lag combination as a change metric. The method was also used to detect new settlement developments in both provinces (section 6.3.2 and 6.4.2). Both these methods were compared to a recently published change detection method that uses NDVI differencing to determine land-cover change. The performance of this method is also given for both provinces (section 6.3.3 and 6.4.3).

It was found that the EKF change detection method performed best in the Limpopo province. This was attributed to the fact that most of the province is covered by natural vegetation which resulted in a high correlation between the EKF derived parameter sequences of neighboring pixels in a typical 3×3 pixel grid. The neighboring pixel parameter sequences could thus be utilized when calculating the change metric. Even though the settlements are low density and have a high component of vegetation, the relative difference in the EKF parameter steams of the change pixel and its neighboring pixels was high enough to detect change. In the Gauteng province the performance of the EKF method was lower. This was attributed to the land-cover diversity that is typical to this province; the 3×3 pixel grid was not as highly correlated as in the Limpopo province, which translated into a subsequent

performance degradation. It is concluded that EKF change detection can effectively exploit the additional information provided by neighboring pixels when the area that is considered is relatively homogeneous for a typical 2.25 km^2 area and the number of contiguous pixels having changed is limited to 4 or 5.

It was found that the temporal ACF change detection method had the best performance in the Gauteng province. The non-stationarity of the change pixels relative to the no-change pixel time-series was effectively exploited. The method considered a single pixel time-series as opposed to a grid of pixels as in the EKF change detection method and was therefore not influenced by heterogeneity of the pixel grid. It was shown that the change detection accuracy of the temporal ACF method is at a maximum when the change date is at the center of the time-series and slightly compromised as the change date moves towards the beginning or end of the time-series. However, the method was able to achieve more than an 80% detection accuracy in both provinces. It is concluded that the temporal ACF change detection method is very robust as it only considers the ACF of a single pixel time-series and is not dependent on the homogeneity of the considered area. The timing of the change should, however, also be considered when most of the change is anticipated to be at the end or start of the time-series. Both the proposed methods performed well for both provinces when compared to a simple NDVI differencing method.